J. Appl. Comput. Mech., 6(3) (2020) 617-639
DOI: 10.22055/JACM.2019.28993.1532

ISSN: 2383-4536
jacm.scu.ac.ir

M&MoCS
Shahid Chamran University of Ahvaz

Journal of
Applied and Computational Mechanics

Research Paper

On the Six Node Hexagon Elements for Continuum Topology Optimization of Plates Carrying in Plane Loading and Shell Structures Carrying out of Plane Loading

K.N.V. Chandrasekhar[1], V. Bhikshma[2], S. Abdul Mohi[1]

[1] CVR College of Engineering, Hyderabad, Telangana, India
[2] Department of Civil Engineering, Osmania University, Hyderabad, Telangana, India

Received March 24 2019; Revised June 24 2019; Accepted for publication June 24 2019.
Corresponding author: K.N.V. Chandrasekhar (Biml.koralla1@gmail.com)

Abstract. The need of polygonal elements to represent the domain is gaining interest among structural engineers. The objective is to perform static analysis and topology optimization of a given continuum domain using the rational fraction type shape functions of six node hexagonal elements. In this paper, the main focus is to perform the topology optimization of two-dimensional plate structures using Evolutionary Swarm Intelligence Firefly Algorithms (ESIFA) and three-dimensional shell structures using optimality criteria. The optimization of plates carrying in plane loading is performed with minimum weight as objective. Two different types of shell structures are optimized using maximum strain energy as criteria. The optimal distribution of the material in the design domain obtained using six node hexagon elements is compared with the optimal distribution of material obtained using quadrilateral elements. A few problems from the literature have been solved and this study has proved that hexagon element gives better results over traditional quadrilateral elements.

Keywords: Six node hexagon, Topology, Shells, Firelfy algorithms, Strain energy optimization, Weight optimization.

1. Introduction

The partial differential equations are useful to accurately formulate the problems of structural mechanics, electromagnetics, fracture, propagation of heat and sound, fluid flow and elasticity. It is well established that the triangular or quadrilateral elements were traditionally used to represent the domains. Sometimes it is very difficult to represent the domain using these elements and the need for a suitable element arises. Polygonal elements are one such great opportunity to model a multi-scale physical nature of the problem [1]. In his paper, the rational fraction type shape functions were proposed by Misako [2] was used to perform the structural analysis and perform topology optimization. Singh [1] has developed integration schemes for polygonal finite element method with Schwarz conformal mapping. In his study, he uses Wachpress shape functions to analyze the cantilever subjected to pure shear and pure axial tensile loads. He used pentagon and hexagon elements to analyze the structure. The pentagon and hexagon are represented by using five triangles and 79 integration points were used per triangle. The convergence in the strain energy versus the number of nodes was studied in detail. The extended finite element method based formulation is applied to analyze the plate having an edge crack under uniaxial loading. A comparison of convergence of stress intensity factors is studied between the responses with the quadrilateral mesh and the hexagonal mesh.

Published online: September 24 2019

The need for further analysis of continuum structures carrying different types of loading, geometry and boundary conditions arises. The optimization of the continuum domain can be performed using different methods. In this paper, the main focus is to check the compatibility of hexagon elements when used for different domains and loading conditions along with different kinds of optimization algorithms. Four different problems are solved and presented in this paper. The first two problems are plate structure carrying in-plane loading and the next two problems are shell structures carrying out-of-plane loading. The first problem is a static analysis problem of a rectangular domain meshed using hexagon elements. The results of nodal displacements using hexagonal mesh are compared with the nodal displacements obtained when the same domain is meshed using four node quadrilateral elements. The results from the static analysis are symmetrical. The second problem is a case of a two-dimensional rectangular plane carrying in-plane loading. The topology optimization is performed with minimum weight as objective using ESIFA. The distribution obtained is quite similar to the distribution obtained by meshing the continuum using quadrilateral elements. The optimization results have shown that the hexagon elements interlock each other well when compared with other elements and hence the nodal displacements are lower than the maximum nodal displacements obtained when using traditional quadrilateral elements to discretize the same domain. The study of shell structures in engineering has been increasing at a remarkable rate. The third problem is a shell structure carrying out-of-plane loading. A new grid-based method is used to perform topology optimization of shell structures where in the sine curve pattern is adopted to identify the elements in the neighborhood to prepare a grid for each element. The elements in the design domain are edge connected and hence by the nature of the geometry of the hexagon, the elements are aligned along a curved line. The topology optimization is performed with maximization of strain energy as the objective and using optimality criteria as the optimization method. The fourth problem is the strain energy optimization of the shell structure. The Topology optimization is performed using optimality criteria. The distribution of the material is quite similar to the distribution of material obtained using quadrilateral elements. The unique nature of the element is showing a patch behavior which is identified and discussed. The coding is done using C and Matlab. The results obtained using hexagonal mesh is compared with those results existing in the literature. The results are encouraging and have shown that the hexagon element is quite stable.

Michel [3] in his paper developed a semi-lagrangian solver for the Vlasov-Poisson equation on a uniform hexagonal mesh. Talischi [4] investigated Wachpress type hexagonal elements and present their implementation to perform Topology optimization using three methods, element based, continuous approximation of the distribution of the material, and minimum length scale through projection functions. Verners [5] studied the correlation between the static and dynamic stiffness of the super element of hexagonal structure. Huang et al. [6] in their study on Honey Comb core showed that Honey comb has good Stiffness and also less Relative Density, because of which good amount of work had been done on them in order to use them in engineering applications for the last few years as core material in structures. Modelling of the Honeycomb is done by using two theories namely beam theory and solid theory. In beam theory the Relative density is low and with uniform double wall thickness of the core. In solid theory model the relative density is high. Optimal condition is derived by using the maximum Eigen value method and by using the Fourth-order differential equation for shells, plates, and columns. The authors [7] have proposed a variable cylindrical shell which can carry the stresses developed in the material effectively. Zienkiewicz is the first to use Finite Element in the shape optimization of the structure and where on the work on Shape and sizing optimization had begun. A good, and efficient design of the structures needs minimum execution time, less cost, less displacement, min acceleration, and so on. When all of such criteria need to be considered, designing is a quite complicated task and hence require an automated process to perform optimization. Falco et al. [8] in their study on plates and shells have considered dynamic loading for the calculation of the optimal design. They performed the Shape and Sizing optimization which include the generation of the Surface, mesh, Analysis consisting of finite element, sensitivity, using the Sequential quadratic Algorithm to perform optimization of the long, short cylindrical shells, and square plates subjected to impulse, and harmonic loading. Khoza [9] performed Topology optimization of shells structures and plates with the micro structures, by using the optimality criterion, moving asymptotes method as the algorithm in optimization. Using the Kirchoff (shear rigid), Mindlin (shear flexible) plate elements, finite element formulation is done and also the behavior of the elements are studied on the optimization, and a discrete Kirchoff quadrilateral plate element with different support condition, including poisons ratio and more penalty factor, is presented. A Scordelis-Lo roof which has a single curvature and also gives a composite kinematic performance, is selected as custom problem with and without stiffeners, different aspect ratio, and different volume fractions are studied [9].

Ivana [10] has studied the non-linear and linear buckling analysis with material and geometric imperfection for the existing shells structures which were analyzed before the existence of the computers and FEM, using the methods of approximates for the analysis. Later, using the sofiplus as a tool, modelling the structure, generation of the mesh using the Q4, T3 elements is done in the Finite Element Analysis package called Sofistik, which can do the structural analysis and as well as the optimization for a large domain considering the geometry of the members, boundary condition, material used, position for the location of the steel and under various kinds of the loading. Tao Yin [11] has studied a definite length Cylindrical Circular Shell having a crack on the circumference is selected and a Dynamic Analysis is done to know the dynamic behavior using four different sets of support conditions which result in a unique solution. The numerical methods are applied in this study and it had also been proved that the formulation is independent on the boundary conditions.

Awad et al. [12] have considered the spherical shell for performing optimal analysis and optimization. Method of integral equation is used for the development of the governing equation because it requires fewer amounts of data for input, hybrid approach, less codeal line because of which it is also called a computationally dynamic method. In order to apply the method in the engineering i.e., especially in the shell analysis a model is selected with two different types of the construction i.e., the shell having constant and varying thickness is taken and the results are verified by the using the FEA and numerical methods wherever required. Weight of the structure is reduced by introducing a penalty function with stresses, displacements as variables. Aswini [13] performed the analysis of cylindrical roof shell in two different cases i.e., shell having the edge beam and the other shell not having the edge beams. The computer based analysis is done by adopting the Matlab software. Furthermore short shell and long shell with both the cases are analyzed using the Beam membrane theory, and analytical methods available are used for the soft analysis. Various stress parameters are estimated with the change in the length of the shell and the semi-central angle. Ahmad [14] performed analysis of shell structures by using elements which have a defined geometry i.e., example a triangle with all the straight edges, and other with all the edges as curved edges. The analysis of shell structure is performed for two types of thickness i.e., a thin shell and a thick shell. A new curved shell had been formulated irrespective of the geometry and by avoiding the deformation caused due to shear. Shells having the symmetric axis of rotations and loading act symmetrically (e.g. spherical domes) and non-symmetric loading (e.g. cooling tower) were solved.

In Section 2, the existing work done by several authors on optimization of plates and shells is reviewed. Section 3 discusses briefly the theoretical background and the governing equations required. The flowcharts showing the process to perform the topology optimization are presented here. Section 4 presents the approach followed and process flowcharts used to conduct this study. In section 5, the objective function for each type of problems for plates and shells are given. In section 6, the analysis is done here, four different problems on static analysis, plates carrying in-plane loading with weight minimization, shells carrying out-of-plane loading with strain energy optimization are discussed here. In section 7, the conclusions of this study are presented here. The references are given at the end. In appendix A, the calculations to determine the length of the arc for the shell structure are given.

1.1 Objectives of the study

- To perform the static analysis of continuum structures using six node hexagonal elements
- To perform the topology optimization of continuum structures of plates and shells

1.2 Scope of the study

- The study is performed within the linear static elastic limits only
- Hooke's law is valid
- The study does not include buckling analysis

2. Theoretical Background

2.1 Rational fraction type Shape functions [2]

Rational fraction type shape functions for six node hexagon element (honey beehive element) are given below. Fig.1 shows the unit cell of the hexagon element.

The shape functions are as follows given in Eq. (1).

$$
\begin{aligned}
v &= 2\left(3-x^2-y^2\right)\\
N_1 &= \frac{1}{v}\left(1-\frac{2y}{\sqrt{3}}\right)\left(1+x-\frac{y}{\sqrt{3}}\right)\left(1+x+\frac{y}{\sqrt{3}}\right)\left(1+\frac{2y}{\sqrt{3}}\right)\\
N_2 &= \frac{1}{v}\left(1+x-\frac{y}{\sqrt{3}}\right)\left(1+x+\frac{y}{\sqrt{3}}\right)\left(1+\frac{2y}{\sqrt{3}}\right)\left(1-x+\frac{y}{\sqrt{3}}\right)\\
N_3 &= \frac{1}{v}\left(1+x+\frac{y}{\sqrt{3}}\right)\left(1+\frac{2y}{\sqrt{3}}\right)\left(1-x+\frac{y}{\sqrt{3}}\right)\left(1-x-\frac{y}{\sqrt{3}}\right)\\
N_4 &= \frac{1}{v}\left(1+\frac{2y}{\sqrt{3}}\right)\left(1-x+\frac{y}{\sqrt{3}}\right)\left(1-x-\frac{y}{\sqrt{3}}\right)\left(1-\frac{2y}{\sqrt{3}}\right)\\
N_5 &= \frac{1}{v}\left(1-x+\frac{y}{\sqrt{3}}\right)\left(1-x-\frac{y}{\sqrt{3}}\right)\left(1-\frac{2y}{\sqrt{3}}\right)\left(1+x-\frac{y}{\sqrt{3}}\right)\\
N_6 &= \frac{1}{v}\left(1-x-\frac{y}{\sqrt{3}}\right)\left(1-\frac{2y}{\sqrt{3}}\right)\left(1+x-\frac{y}{\sqrt{3}}\right)\left(1+x+\frac{y}{\sqrt{3}}\right)
\end{aligned}
\tag{1}
$$

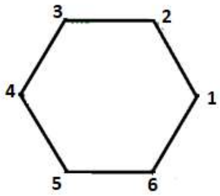

Fig. 1. The Unit cell of six node hexagon element

2.2 Formulation of thin shells [15]

The formulation of the shell roof is done using degen element with five degrees of freedom per node as shown in the Fig.2. There are eight significant strains over the mid surface. The generalized strain vector and displacement vector correspond to the mid-surface. The governing equations of thin shells are summarized below [15]

2.2.1 Assumptions

1. The stresses normal to the surface in the z-direction is equal to zero, $\sigma_z = 0$

2. The material is homogeneous and obeys Hooke's Law.

There are eight strain components at any point is as given in Eq. (2):

$$\begin{aligned} \varepsilon_{xa} &= \varepsilon_{xoa} + zk_{xa} \\ \varepsilon_{ya} &= \varepsilon_{yoa} + zk_{ya} \\ \varepsilon_{za} &= \varepsilon_{zoa} = 0 \\ \gamma_{xya} &= \gamma_{xyoa} + zk_{xy} \\ \gamma_{yza} &= \varphi_x \\ \gamma_{zxa} &= \varphi_y \end{aligned} \tag{2}$$

where the mid-surface strains are defined as follows as given in Eq. (3):

$$\begin{aligned} \varepsilon_{xo\alpha} &= \frac{\partial u_{o\alpha}}{\partial x_\alpha} \\ \varepsilon_{yo\alpha} &= \frac{\partial v_{o\alpha}}{\partial y_\alpha} \\ \varepsilon_{xyo\alpha} &= \frac{\partial u_{o\alpha}}{\partial y_\alpha} + \frac{\partial v_{o\alpha}}{\partial x_\alpha} \\ k_{x\alpha} &= \frac{\partial \theta_{y\alpha}}{\partial x_\alpha} \\ k_{y\alpha} &= -\frac{\partial \theta_{x\alpha}}{\partial y_\alpha} \\ k_{xy\alpha} &= \frac{\partial \theta_{y\alpha}}{\partial y} - \frac{\partial \theta_{x\alpha}}{\partial x} \\ \varphi_x &= \frac{\partial w_{o\alpha}}{\partial y_\alpha} - \theta_{x\alpha} \\ \varphi_y &= \frac{\partial w_{o\alpha}}{\partial x_\alpha} - \theta_{y\alpha} \end{aligned} \tag{3}$$

The strain vector and displacement vector corresponding to the mid-surface [16] are given in Eq. (4):

$$\bar{\boldsymbol{\varepsilon}}_{\boldsymbol{\alpha}} = [\boldsymbol{\varepsilon}_{xo\boldsymbol{\alpha}},\ \boldsymbol{\varepsilon}_{yo\boldsymbol{\alpha}},\ \boldsymbol{\varepsilon}_{xyo\boldsymbol{\alpha}},\ k_{x\boldsymbol{\alpha}},\ k_{y\boldsymbol{\alpha}},\ k_{xy\boldsymbol{\alpha}},\ \boldsymbol{\varphi}_x,\ \boldsymbol{\varphi}_y\ ]^T \tag{4}$$

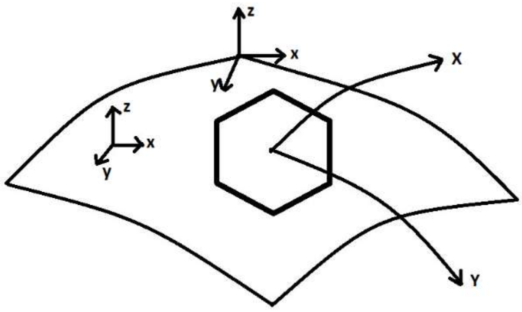

Fig. 2. The element Local and Global coordinates axis for the domain

The displacement vector corresponding to the strain vector is given by Eq. (5):

$$\mathbf{d}_\alpha = (u_{xo\alpha},\ v_{yo\alpha},\ w_{zo\alpha},\ \theta_{x\alpha},\ \theta_{y\alpha})^T \tag{5}$$

The constitutive relation is given in Eq. (6) below:

$$\boldsymbol{\sigma}_{\alpha i} = \mathbf{C}_{ij}\boldsymbol{\varepsilon}_{\alpha j} \quad j = 1,2,3,4,5 \tag{6}$$

The coefficients C_{ij} constitute the isotropic material stiffness matrix and is given in Eq. (7) as follows:

$$\mathbf{C}_{ij} = \begin{bmatrix} \frac{E}{(1-\nu\nu)} & \frac{\nu E}{(1-\nu\nu)} & 0 & 0 & 0 \\ \frac{\nu E}{(1-\nu\nu)} & \frac{E}{(1-\nu\nu)} & 0 & 0 & 0 \\ 0 & 0 & \frac{E}{2(1+\nu)} & 0 & 0 \\ 0 & 0 & 0 & \frac{E}{2(1+\nu)} & 0 \\ 0 & 0 & 0 & 0 & \frac{E}{2(1+\nu)} \end{bmatrix} \tag{7}$$

The stress vector is given by Eq. (8):

$$\boldsymbol{\sigma}_\alpha = (\sigma_{x\alpha},\ \sigma_{y\alpha},\ \tau_{xy\alpha},\ \tau_{yz\alpha},\ \tau_{zx\alpha})^T \tag{8}$$

The strain vector is given by Eq. (9):

$$\boldsymbol{\varepsilon}_\alpha = (\varepsilon_{x\alpha},\ \varepsilon_{y\alpha},\ \varepsilon_{xy\alpha},\ \gamma_{yz\alpha},\ \gamma_{zx\alpha})^T \tag{9}$$

Stress resultants at the middle surface can be derived using the potential energy expression as follows in Eq. (10):

$$U = \frac{1}{2}\int_\Omega \boldsymbol{\varepsilon}_\alpha^T \boldsymbol{\sigma}_\alpha \, d\Omega$$

$$U = \frac{1}{2}\int \left[\sigma_{x\alpha}(\varepsilon_{xo\alpha} + z_\alpha k_{x\alpha}) + \sigma_{y\alpha}(\varepsilon_{yo\alpha} + z_\alpha k_{y\alpha}) + \tau_{xy\alpha}(\varepsilon_{xyo\alpha} + z_\alpha k_{xy\alpha}) + \tau_{yz\alpha}\varphi_x + \tau_{xz\alpha}\varphi_y\right] dAdz \tag{10}$$

$$U = \frac{1}{2}\int \left[(\varepsilon_{xo\alpha}N_{x\alpha} + N_{y\alpha}\varepsilon_{yo\alpha} + N_{xy\alpha}\varepsilon_{xyo\alpha} + M_{x\alpha}k_{x\alpha} + M_{y\alpha}k_{y\alpha} + M_{xy\alpha}k_{xy\alpha} + Q_{x\alpha}\varphi_{x\alpha} + Q_{y\alpha}\varphi_{y\alpha}\right] dA$$

The stress resultants at the mid surface are given in Eq. (11) below:
Extensional force:

$$N_{x\alpha} = \int_{-t_\alpha/2}^{t_\alpha/2} \sigma_{x\alpha}\, dz \tag{11a}$$

Extensional force:

$$N_{y\alpha} = \int_{-t_\alpha/2}^{t_\alpha/2} \sigma_{y\alpha}\, dz \tag{11b}$$

In plane shear force:

$$N_{xy\alpha} = \int_{-t_\alpha/2}^{t_\alpha/2} \tau_{xy\alpha}\, dz \tag{11c}$$

Bending moment:

$$M_{x\alpha} = \int_{-t_\alpha/2}^{t_\alpha/2} \sigma_{x\alpha}\, z_\alpha\, dz \tag{11d}$$

Bending moment:

$$M_{y\alpha} = \int_{-t_\alpha/2}^{t_\alpha/2} \sigma_{y\alpha}\, z_\alpha\, dz \tag{11e}$$

In plane twisting moment:

$$M_{xy\alpha} = \int_{-t_\alpha/2}^{t_\alpha/2} \tau_{xy\alpha}\, z_\alpha\, dz \tag{11f}$$

Transverse shear forces:

$$Q_{x\alpha} = \int_{-t_\alpha/2}^{t_\alpha/2} \tau_{yz\alpha}\, dz \tag{11g}$$

Transverse shear force:

$$Q_{y\alpha} = \int_{-t_\alpha/2}^{t_\alpha/2} \tau_{xz\alpha}\, dz \tag{11h}$$

Here $N_{x\alpha}$, $N_{y\alpha}$, $N_{xy\alpha}$, $M_{x\alpha}$, $M_{y\alpha}$, $M_{xy\alpha}$, $Q_{x\alpha}$, $Q_{y\alpha}$ are the stress resultants at the mid-surface $N_{x\alpha}$, $N_{y\alpha}$ are extensional forces, $Q_{x\alpha}$, $Q_{y\alpha}$ are transverse shear forces $M_{x\alpha}$, $M_{y\alpha}$ are bending moments, $N_{xy\alpha}$, $M_{xy\alpha}$ are the in-plane shear forces and twisting moments respectively. After carrying out the integration in the thickness direction, we have given in Eq. (12):

$$\begin{aligned} N_{\boldsymbol{\alpha}} &= \bar{\mathbf{D}}_{m\boldsymbol{\alpha}} \bar{\boldsymbol{\varepsilon}}_{\boldsymbol{\alpha}} \\ M_{\boldsymbol{\alpha}} &= \bar{\mathbf{D}}_{b\boldsymbol{\alpha}} \bar{\boldsymbol{\varepsilon}}_{\boldsymbol{\alpha}} \\ Q_{\boldsymbol{\alpha}} &= \bar{\mathbf{D}}_{s\boldsymbol{\alpha}} \bar{\boldsymbol{\varepsilon}}_{\boldsymbol{\alpha}} \end{aligned} \tag{12}$$

where $\bar{\mathbf{D}}_{m\alpha}$, $\bar{\mathbf{D}}_{b\alpha}$, $\bar{\mathbf{D}}_{s\alpha}$ are the membrane, flexural and shear rigidity matrices given as follows in Eq. (13):

$$\bar{\mathbf{D}}_{m\alpha} = \begin{bmatrix} \frac{Et_\alpha}{(1-\nu\nu)} & \frac{\nu Et_\alpha}{(1-\nu\nu)} & 0 & 0\,0\,0\,0\,0 \\ \frac{\nu Et_\alpha}{(1-\nu\nu)} & \frac{Et_\alpha}{(1-\nu\nu)} & 0 & 0\,0\,0\,0\,0 \\ 0 & 0 & \frac{Et_\alpha}{2(1+\nu)} & 0\,0\,0\,0\,0 \end{bmatrix} \tag{13a}$$

$$\bar{\mathbf{D}}_{b\alpha} = \begin{bmatrix} 0 & 0 & 0 & \frac{Et_\alpha{}^3}{12(1-\nu\nu)} & \frac{\nu Et_\alpha{}^3}{12(1-\nu\nu)} & 0 & 0 & 0 & 0 \\ 0 & 0 & 0 & \frac{\nu Et_\alpha{}^3}{12(1-\nu\nu)} & \frac{Et_\alpha{}^3}{12(1-\nu\nu)} & 0 & 0 & 0 & 0 \\ 0 & 0 & 0 & 0 & 0 & \frac{Et_\alpha{}^3}{24(1+\nu)} & 0 & 0 & 0 \end{bmatrix} \tag{13b}$$

$$\bar{\mathbf{D}}_{s\alpha} = \begin{bmatrix} 0 & 0 & 0 & 0 & 0 & 0 & \dfrac{Et_\alpha}{24(1+\nu)} & 0 \\ 0 & 0 & 0 & 0 & 0 & 0 & 0 & \dfrac{Et_\alpha}{24(1+\nu)} \end{bmatrix} \tag{13c}$$

$$\bar{\sigma}_\alpha = \begin{bmatrix} N_\alpha \\ M_\alpha \\ Q_\alpha \end{bmatrix} = \begin{bmatrix} \bar{D}_{m\alpha} & 0 & 0 \\ 0 & \bar{D}_{b\alpha} & 0 \\ 0 & 0 & \bar{D}_{s\alpha} \end{bmatrix} \bar{\varepsilon}_\alpha = \bar{\mathbf{D}}_\alpha \bar{\varepsilon}_\alpha \tag{13d}$$

we define,

$$\begin{aligned} \bar{\varepsilon}_{m\alpha} &= \mathbf{L}_{m\alpha} d_\alpha \\ \bar{\varepsilon}_{b\alpha} &= \mathbf{L}_{b\alpha} d_\alpha \\ \bar{\varepsilon}_{s\alpha} &= \mathbf{L}_{s\alpha} d_\alpha \end{aligned} \tag{13e}$$

Here $\mathbf{L}_{m\alpha}$ $\mathbf{L}_{b\alpha}$ $\mathbf{L}_{s\alpha}$ are the strain operator matrices in the membrane, bending, and shear respectively given as follows in Eq. (14):

$$\mathbf{L}_{m\alpha} = \begin{bmatrix} \dfrac{\partial}{\partial x_\alpha} & 0 & 0 & 0 & 0 \\ 0 & \dfrac{\partial}{\partial y_\alpha} & 0 & 0 & 0 \\ \dfrac{\partial}{\partial y_\alpha} & \dfrac{\partial}{\partial x_\alpha} & 0 & 0 & 0 \end{bmatrix}$$

$$\mathbf{L}_{b\alpha} = \begin{bmatrix} 0 & 0 & 0 & 0 & \dfrac{\partial}{\partial x_\alpha} \\ 0 & 0 & 0 & \dfrac{-\partial}{\partial y_\alpha} & 0 \\ 0 & 0 & 0 & \dfrac{-\partial}{\partial x_\alpha} & \dfrac{\partial}{\partial y_\alpha} \end{bmatrix} \tag{14}$$

$$\mathbf{L}_{s\alpha} = \begin{bmatrix} 0 & 0 & \dfrac{\partial}{\partial x_\alpha} & 0 & 1 \\ 0 & 0 & \dfrac{\partial}{\partial y_\alpha} & -1 & 0 \end{bmatrix}$$

Displacement function

The nodal and generalized displacement vectors are related with the shape functions as in Eq. (15):

$$\mathbf{d}_\alpha = \begin{bmatrix} u_{o\alpha} \\ v_{o\alpha} \\ w_{o\alpha} \\ \theta_{x\alpha} \\ \theta_{y\alpha} \end{bmatrix} = \sum_{i=1}^{NN=6} \begin{bmatrix} N_i & 0 & 0 & 0 & 0 \\ 0 & N_i & 0 & 0 & 0 \\ 0 & 0 & N_i & 0 & 0 \\ 0 & 0 & 0 & N_i & 0 \\ 0 & 0 & 0 & 0 & N_i \end{bmatrix} \begin{bmatrix} u_{i\alpha} \\ v_{i\alpha} \\ w_{i\alpha} \\ \theta_{ix\alpha} \\ \theta_{iy\alpha} \end{bmatrix} = \sum_{i=1}^{NN=6} N_i d_{i\alpha} \tag{15}$$

Let the displacement at node *i* in the nodal coordinate system be as given in Eq. (16):

$$\mathbf{d}_{in} = \left(u_{on}\ v_{on}\ w_{on}\ \theta_{xn}\ \theta_{yn} \right)^T \tag{16}$$

Using a transformation matrix $R_{i\alpha}$ is given by Eq. (17):

$$d_{i\alpha}=\mathbf{R}_{\alpha i}\mathbf{d}_{in} \quad \text{where } \mathbf{R}_{\alpha i}=\begin{bmatrix} i_\alpha i_n & i_\alpha j_n & i_\alpha k_n & 0 & 0 \\ j_\alpha i_n & j_\alpha j_n & j_\alpha k_n & 0 & 0 \\ k_\alpha i_n & k_\alpha j_n & k_\alpha k_n & 0 & 0 \\ 0 & 0 & 0 & i_\alpha i_n & i_\alpha j_n \\ 0 & 0 & 0 & j_\alpha i_n & j_\alpha j_n \end{bmatrix} \tag{17}$$

in which N denotes the shape function matrix as shown in Eq. (18):

$$\mathbf{N}=\sum_{i=1}^{NN=6}\begin{bmatrix} N_i & 0 & 0 & 0 & 0 \\ 0 & N_i & 0 & 0 & 0 \\ 0 & 0 & N_i & 0 & 0 \\ 0 & 0 & 0 & N_i & 0 \\ 0 & 0 & 0 & 0 & N_i \end{bmatrix}$$

$$\mathbf{R}=diag[R_{\alpha 1} \dots R_{\alpha i} \dots R_{\alpha 6}] \tag{18}$$

$$d_\alpha=\sum_{i=1}^{NN=6}N_i R_{\alpha i} d_{in}=\mathbf{NRd}_n$$

$$\mathbf{d}_n{}^T=\left[u_1\ v_1\ w_1\ \theta_{x1}\ \theta_{y1} \dots u_{in}\ v_{in}\ w_{in}\ \theta_{xin}\ \theta_{yin} \dots u_6\ v_6\ w_6\ \theta_{x6}\ \theta_{y6}\right]^T$$

Strain displacement matrix is given in Eq. (19):

$$\bar{\varepsilon}_{m\alpha}=\mathbf{L}_{m\alpha}\mathbf{d}_\alpha=\mathbf{L}_{m\alpha}\sum_{i=1}^{NN=6}\mathbf{N}_i\mathbf{d}_{i\alpha}=\mathbf{L}_{m\alpha}\sum_{i=1}^{NN=6}\mathbf{N}_i\mathbf{R}_{i\alpha}\mathbf{d}_{in}=\sum_{i=1}^{6}\mathbf{B}_{mi\alpha}\mathbf{R}_{i\alpha}d_{in}=\sum_{i=1}^{6}\mathbf{B}^*_{mi}\mathbf{d}_{in}=\mathbf{B}^*_m d_n$$

$$\bar{\varepsilon}_{b\alpha}=\mathbf{B}^*_b\mathbf{d}_n \tag{19a}$$

$$\bar{\varepsilon}_{s\alpha}=\mathbf{B}^*_s\mathbf{d}_n$$

where B^*_m, B^*_b, B^*_s are the strain matrices of the membrane, bending and shear displacements respectively.

$$\bar{\varepsilon}_\alpha=\mathbf{B}^*\mathbf{d}_n$$

$$\mathbf{B}^*=\left[B^*_m, B^*_b, B^*_s\right]^T \tag{19b}$$

2.2.2 Isoparametric representation

The geometry and displacements are interpreted using the same shape functions. The space coordinates can be expressed as shown in Eq. (20):

$$\begin{bmatrix} x \\ y \end{bmatrix}=\sum_{i=1}^{NN}\begin{bmatrix} N_i & 0 \\ 0 & N_i \end{bmatrix}\begin{bmatrix} x_i \\ y_i \end{bmatrix} \tag{20}$$

The Jacobian matrix relates the area integral in coordinate x_α and y_α to that in the r and s coordinate system and is given by Eq. (21):

$$\mathbf{J}=\begin{vmatrix} \dfrac{\partial x_\alpha}{\partial r} & \dfrac{\partial y_\alpha}{\partial r} \\ \dfrac{\partial x_\alpha}{\partial s} & \dfrac{\partial y_\alpha}{\partial s} \end{vmatrix}=\begin{vmatrix} l_{1\alpha}\dfrac{\partial X}{\partial r}+m_{1\alpha}\dfrac{\partial Y}{\partial r}+n_{1\alpha}\dfrac{\partial Z}{\partial r} & l_{2\alpha}\dfrac{\partial X}{\partial r}+m_{2\alpha}\dfrac{\partial Y}{\partial r}+n_{2\alpha}\dfrac{\partial Z}{\partial r} \\ l_{1\alpha}\dfrac{\partial X}{\partial s}+m_{1\alpha}\dfrac{\partial Y}{\partial s}+n_{1\alpha}\dfrac{\partial Z}{\partial s} & l_{2\alpha}\dfrac{\partial X}{\partial s}+m_{2\alpha}\dfrac{\partial Y}{\partial s}+n_{2\alpha}\dfrac{\partial Z}{\partial s} \end{vmatrix} \tag{21a}$$

where $l_{1\alpha}, m_{1\alpha}, n_{1\alpha}$ and $l_{2\alpha}, m_{2\alpha}, n_{2\alpha}$ are the direction cosines of the local i_α, j_α axes with respect to the global *i, j, k* respectively. An elemental area on the mid surface is given as:

$$\int_A dA=\int_A dx_\alpha dy_\alpha=\int_{-1}^{1}\int_{-1}^{1}|J|drds \tag{21b}$$

Elemental Stiffness Matrix:

$$\mathbf{K}^e = \int_A \mathbf{B}^{*T}\mathbf{D}_\alpha^e \mathbf{B}^* dA$$
$$\mathbf{K}^e = \mathbf{K}_m^e + \mathbf{K}_b^e + \mathbf{K}_s^e \tag{22a}$$

where

$$\mathbf{K}_m^e = \int_{-1}^{1}\int_{-1}^{1} \mathbf{B}_m^{*T}\mathbf{D}_{m\alpha}\mathbf{B}_m^* |\mathbf{J}| drds = \sum_{\beta=1}^{GP} w_1 w_2 (B_m^*)_\beta^T (D_{m\alpha})(B_m^*)_\beta |J_\beta|$$
$$\mathbf{K}_b^e = \int_{-1}^{1}\int_{-1}^{1} \mathbf{B}_b^{*T}\mathbf{D}_{b\alpha}\mathbf{B}_b^* |\mathbf{J}| drds = \sum_{\beta=1}^{GP} w_1 w_2 (B_b^*)_\beta^T (D_{b\alpha})(B_b^*)_\beta |J_\beta| \tag{22b}$$
$$\mathbf{K}_s^e = \int_{-1}^{1}\int_{-1}^{1} \mathbf{B}_s^{*T}\mathbf{D}_{s\alpha}\mathbf{B}_s^* |\mathbf{J}| drds = \sum_{\beta=1}^{GP} w_1 w_2 (B_s^*)_\beta^T (D_{s\alpha})(B_s^*)_\beta |J_\beta|$$

The $\mathbf{K}_m^e, \mathbf{K}_b^e, \mathbf{K}_s^e$ matrices are the element Membrane, Bending, and Shear stiffness matrices respectively, NGP is the number of Gauss Points and w_1, w_2 are the weights of Gauss points. The numerical integration can be performed using 3 x 3 Gauss quadrature.
Element Load Vector is as shown in Eq. (23) given below:

$$\mathbf{f}^e = \int_A \mathbf{R}^T \mathbf{N}^T F dA \tag{23}$$

where F is the matrix containing magnitude of forces in each of five degrees of freedom direction. Element Mass Matrix is given by Eq. (24):

$$\mathbf{M}^e = \int_{-1}^{1}\int_{-1}^{1} \mathbf{R}_i^T \mathbf{N}_i^T m \mathbf{N}_j \mathbf{R}_j |\mathbf{J}| drds = \sum_{a=1}^{NGP}\sum_{b=1}^{NGP} w_a w_b R_i^T N_i^T m N_j R_j |J| \quad and\ i,j = 1 \ldots NN \tag{24}$$

where, NGP denotes the number of Gauss points in one direction and w_a, w_b are the corresponding weights. The integration can be performed using 3 x 3 Gauss quadrature rule.

$$\text{Here } m = \begin{bmatrix} I_1 & 0 & 0 & 0 & I_2 \\ 0 & I_1 & 0 & -I_2 & 0 \\ 0 & 0 & I_1 & 0 & 0 \\ 0 & -I_2 & 0 & I_3 & 0 \\ I_2 & 0 & 0 & 0 & I_3 \end{bmatrix} \tag{25a}$$

where,

$$I_1 = \int \rho\, dz$$
$$I_2 = \int \rho z\, dz \tag{25b}$$
$$I_3 = \int \rho z * z\, dz$$

2.2.3 Equation of motion without damping

The finite element equation of motion for one element of the domain is given by [17] in Eq. (26):

$$\mathbf{M}^e d_n^e + \mathbf{K}^e d_n^e = \mathbf{f}_n^e \tag{26}$$

The element equations are assembled to yield the global equation of motion for the entire domain is given in Eq. (27) below:

$$\mathbf{M}\ddot{d} + \mathbf{K}d = \mathbf{f} \tag{27}$$

where, $d, \ddot{d}$ are the global vectors of displacement and acceleration respectively and **M**, **K**, **f** are global mass matrix, global stiffness matrices and nodal load vector given by [18]:

$$
\begin{aligned}
\mathbf{M} &= \sum_{1}^{NE} \mathbf{M}^{e} \\
\mathbf{K} &= \sum_{1}^{NE} \mathbf{K}^{e} \\
\mathbf{f} &= \sum_{1}^{NE} \mathbf{f}^{e}
\end{aligned} \tag{28}
$$

2.3 Connectivity analysis

Figure 3 (a) shows two hexagonal elements connected with one and Fig.3 b displays the hexagonal elements connected by one edge. The node connected elements cannot transfer moment and hence are considered as not connected. The elements in the continuum domain carry moment and shear, can transfer only when the elements are edge connected.

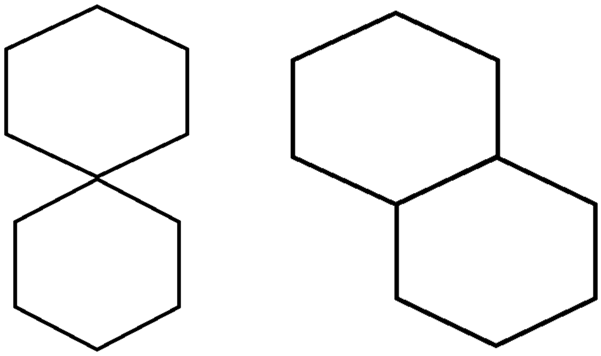

Fig. 3. (a) Not connected **Fig. 3.** (b) Edge Connected

2.3.1 Stress based proportioning [19]

The distribution of material is done based on the stress carried out by the element. In other words, the element carrying more stress will be having a higher density value and the element having lower stress will have a lower density value. The relative density is computed as given in Eq. (29) as

$$
\text{Relative Density} = \frac{\text{maximum principal stress carried by the element}}{\text{maximum principal stress carried by the structure}} \tag{29}
$$

The density value varies in the interval of [0, 1]. This should ensure that the material distribution is done efficiently by identifying the elements which can carry material and the newer configuration of material distribution in the structure can be effectively used to safely transmit the loads.

A Move is counted when one particle, *I*, moves towards the particle, *J*, with lower weight. One Move requires two FE computations. One iteration is complete when all the individuals move towards the other individuals with lower weight. One run has several iterations. A Finite element program developed and is used for performing topology optimization on a computer with Intel I7 processor 4 core, 3.4 GHz with 4 GB RAM is used.

2.4 Introduction to fire fly algorithm

Swarm intelligence algorithms inspired by nature are becoming more popular in solving optimization problems. One of the most recent examples is firefly algorithm which combines levy flights to depict the typical flight characteristics of animals and insects. This algorithm was found to be more promising and superior over many other such algorithms. These search strategies performed using multi agents are efficient in local search and as well as finding global best solutions [20]. The flashing light can be formulated in such a way that it is associated with the objective function to be optimized, which makes it possible to formulate new optimization algorithms.

2.4.1 Assumptions

There are three idealized rules which are the key to this algorithm [21]:

1. All fireflies are unit, which mean that each fly and get attracted to the other.
2. Attractiveness if proportional to their brightness, for any two flashing flies. The less bright fly move towards more bright fly. The attractiveness is proportional to the brightness and they both decrease as their distance increases. If there is no brighter fly it will move randomly.

3. The brightness of the fly is determined by the landscape of the objective function. For a maximization problem, the brightness can simply be proportional to the objective function.

2.4.2 Theory

There are two important issues that have to be dealt with [22]. First one, variation of light intensity and formulation of attractiveness. The brightness/attractiveness is seen in the eyes of the beholder or judged by other flies. It will vary with the distance r_{ij} between firefly *i* and firefly *j*. The light intensity decreases with the distance from its source, and light is also absorbed in the media, with the attractiveness varying with the degree of absorption. The Cartesian distance between the two fireflies *i* and *j* at x_j and x_i is given by [20]:

$$r_{ij} = \sqrt{\sum_{k=1}^{d} \left(x_{i,k} - x_{j,k}\right)^2} \tag{30}$$

where, $x_{i,k}$ is the k^{th} component of the spatial co-ordinate x_i of i^{th} firefly. The movement of the firefly *i* is attracted to another more attractive (brighter) firefly *j* is determined by Eq. (31):

$$x_i = x_i + \beta e^{-\gamma r_{ij}^2}(x_j - x_i) + \alpha \; sign\left[rand - \frac{1}{2}\right] Levy \tag{31}$$

where the second term is due to the attraction and the third term is randomization via levy flights with α being the randomization parameter. The $sign[rand - 1/2]$ where $rand \; \varepsilon \left[0\;1\right]$ essentially provides a random sign or direction while the random step length is drawn from a levy distribution whose mean is infinite and variance is infinite as shown in Eq. (32):

$$\begin{aligned} &Levy \sim u = t^{-\nu}, (1 < \nu \le 3) \\ &Levy\ distribution\ is = \frac{1}{\sqrt{2\Pi}} \frac{e^{-\frac{u}{2}}}{u^{3/2}} \end{aligned} \tag{32}$$

The steps of firefly are drawn from a Levy distribution random walk with a power law step length distribution with a heavy tail.

2.5 Optimality criteria

Siu [23] discussed the theory of optimality criteria. The objective function is weight of the structure or Strain energy is denoted by W. The constraint is given by *C*. The Lagrange equations are written and the optimum values of the unknown variable *A* are determined. The equations are summarized and given below.

Objective function

The objective function can be either to minimize the weight of the structure or to minimize the compliance of the structure. The objective functions for both the cases are given below in Eq. (30) and Eq. (32). Maximize the strain energy of the structure

$$C = \sum_{e=1}^{N} \frac{1}{2} U_e^T \mathbf{K}_e U_e \tag{33}$$

Minimize the weight of the structure:

$$W = \sum_{i=1}^{N} (\rho_i A_i L_i) \tag{34}$$

Constraint:

$$C_j - \bar{C}_j \tag{35}$$

The Lagrange Equation is given by:

$$L_{(A\lambda)} = \sum_{i=1}^{n} (\rho_i A_i L_i) + \sum_{j=1}^{m} \lambda_j (C_j - \bar{C}_j) \tag{36}$$

In which λ_j is the Lagrange multiplier. Differentiating the equation with respect to variable A_i and equating to zero, we have:

$$\lambda_j \ge 0 \tag{37}$$

$$\lambda_j g_j = 0$$

$$\rho_i l_i + \sum_{j=1}^{m} \lambda_j \frac{\partial C_j}{\partial A_j} = 0 \quad (i = 1,\ldots n)$$

$$\frac{1}{\rho_i l_i} \sum_{j=1}^{m} \lambda_j \frac{\partial C_j}{\partial A_j} = -1 \quad (i = 1,\ldots n)$$

The following equation can be obtained as given in Eq. (38):

$$\sum_{j=1}^{m} \lambda_s \left(\sum_{i=1}^{n} \frac{A_i}{\rho_i l_i} \frac{\partial C_j}{\partial A_i} \frac{\partial C_j}{\partial A_i}\right)_r, = -\sum_{i=1}^{n} \left(\frac{\partial C_j}{\partial A_i}\right)_r A_i^r - \eta(\bar{C}_j - C_j^r) \quad (j = 1,\ldots m) \tag{38}$$

3. Methodology

The literature review is performed and the rational fractional type shape functions were used in this study. Static analysis is performed to check for the stability of the element. The stresses and displacements were evaluated. Topology optimization of the plate is performed for two loading conditions. The results for the distribution of material are plotted and the conclusions were made. Figure 4 shows the organization of this manuscript for this study.

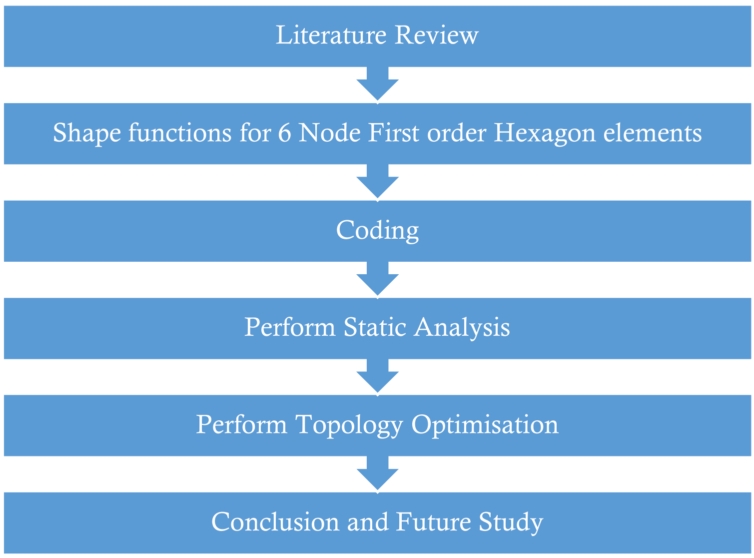

Fig. 4. The organization of this manuscript for this study

3.1 The program

The program consists of two main modules:

a. Finite Element module
b. Optimizer module

3.1.1 Flow chart for optimization using swarm intelligence algorithm

The flow chart to conduct this study is as shown in the Fig. 5 [19].

This process is iterative and until the minimum weight of the structure is reached satisfying all the constraints. A few problems in the literature are solved and the result compared. The fire fly parameters are aggressiveness of random move α= 1.0, attractiveness parameter β =1.0, absorption coefficient γ = 1.0, levy distribution parameter λ= 1.5. The process flow chart is as shown below in Fig. 5.

3.1.2 Using Optimality criteria

The main objective of this study is to perform topology optimization of thin shells. The design domain of the thin shell is discretized using six node hexagon elements. The thin shell formulation is performed using total potential energy concept. This study is focused on degenerative shell elements with the finite element discretization. The number of degrees of freedom per node is taken as five which include translation displacements along x, y, z axis and rotation displacements about the x and y axis as shown in the Fig. 6.

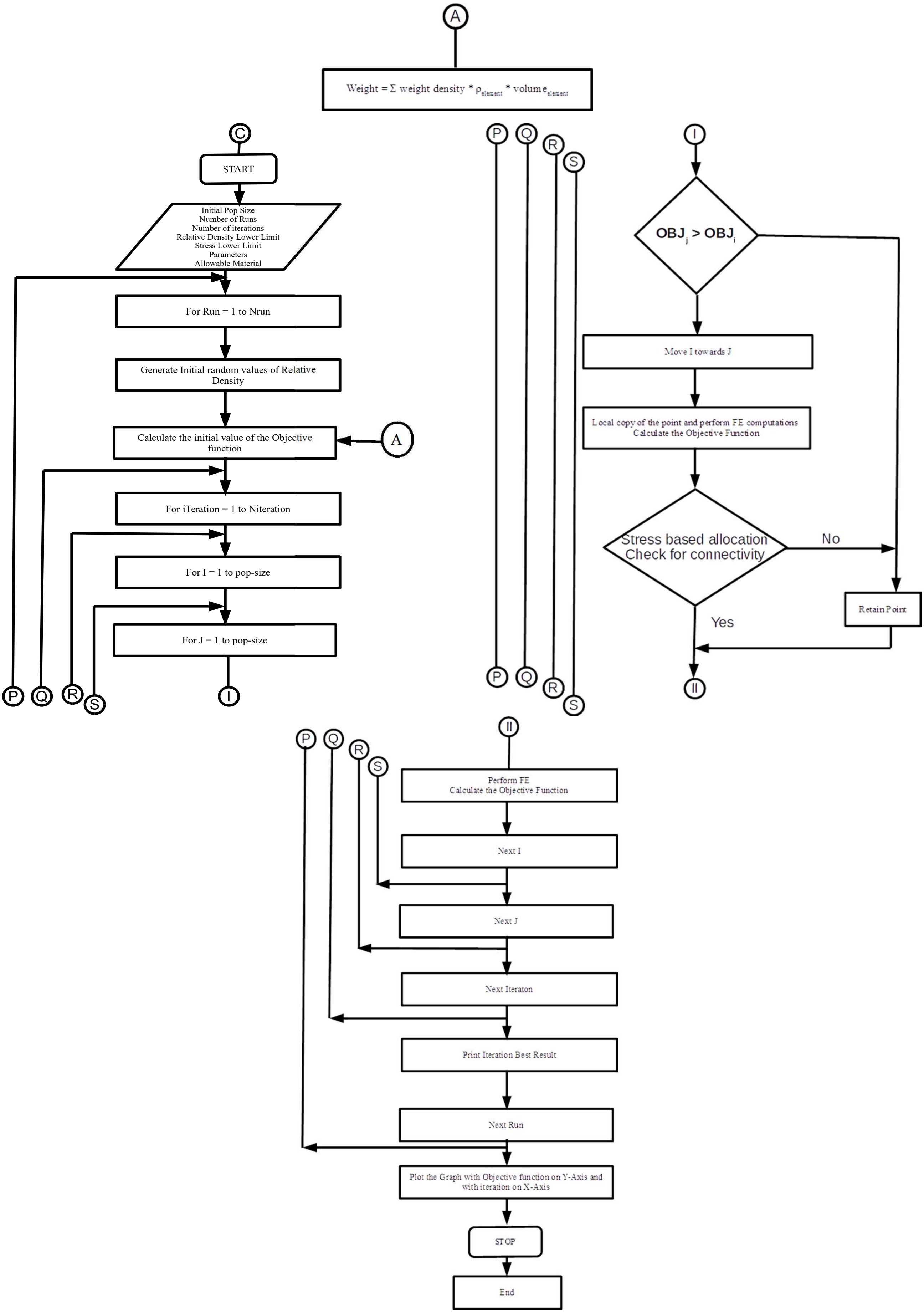

Fig. 5. Flow chart to perform topology optimization using Swarm Intelligence Algorithm

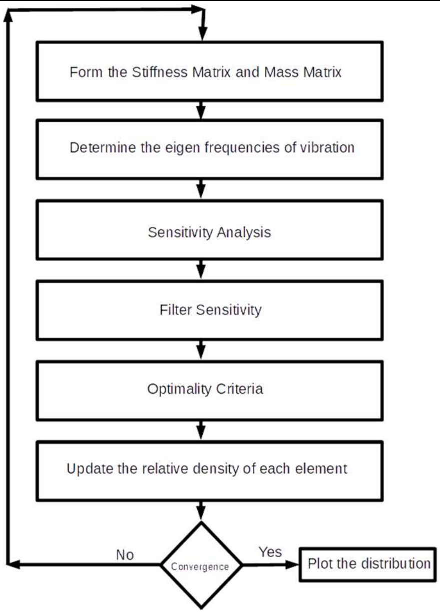

Fig. 6. The flow chart of the optimization module using Optimality criteria

3.2 Grid

Six node hexagonal elements interconnected with an edge in common.The rectangular grid is prepared to identify the neighborhood elements. The hexagonal elements are linked to each other with each edge as shown in the Fig.7. The elements are interconnected with one edge in common with each other as shown in the Fig.7. The geometry gives the hexagonal elements very high strength. The elements are ordered using a sine curve pattern to prepare the grid as shown in Table1.

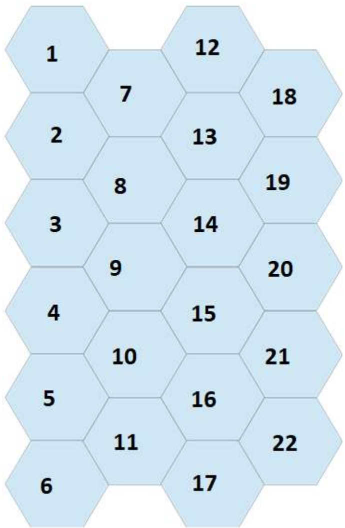

Fig. 7. The six-node hexagonal mesh with the element numbers inside

Table 1. The grid of neighboring elements

1	2	3	4	5	6
7	8	9	10	11	0
12	13	14	15	16	17
18	19	20	21	22	0

1. The grid in x-y plane is prepared which contains the element numbers. As the six node hexagon element has six faces there are six elements surrounding the element which are connected with one edge.
The sine curve pattern is followed to generate the x-y grid which contains all the elements which are connected with having one edge in common along y-axis. The elements along the x-axis are connected by having one edge in common.
2. The number of elements in each row is not equal. The number of elements is arranged alternatively in odd and even numbers. Hence, the last row of elements alternatively has one element less than the other rows. Hence these elements have been taken as zero for the sake of completeness and during optimization process these elements have been excluded.

3. During the optimization of continuum structures there is a transfer of bending moment and shear force between the elements along the edges. The elements which are connected by corner cannot transfer any moment and hence they act as hinges. However, in case of hexagon grid all the elements are connected with one edge in common and hence the vertical displacement for shell structures is substantially lower than the displacements evaluated by taking a rectangular mesh.

4. Objective Function

The topology optimization of the shell structures is then performed using the following objective function

1) Minimizing Weight
2) Maximizing Strain Energy

4.1 Minimizing Weight

The objective is to find the minimum weight of the structure as given by Eq. (39) is subjected to the constraint on the amount of material used and the stresses in the structure:

$$f = (\sum_{i=1}^{n} \rho_i v_i) \times \bar{\rho} \tag{39}$$

where ρ_i is the density parameter of the element, v_i is the volume of the element, and $\bar{\rho}$ is the density of the material subjected to:

$$M \times v - (\sum_{i=1}^{n} \rho_i v_i) \geq 0 \tag{40}$$

where M is the allowable material in percentage, and v is the volume of the structure.
Principal stress:

$$\begin{gathered} \sigma_i \leq \sigma_{allow} \quad i = 1,2,3 \\ 0 \leq \rho_{\min} \leq \rho_e \leq 1 \end{gathered} \tag{41}$$

The Principal stress calculated at the centroid of each element is less than or equal to the allowable principal stress in the material. The relative density of each element should be more than or equal to the minimum relative density and less than or equal to unity.

4.2 Maximizing strain energy

The strain energy of the structure is given by Eq. (42):

$$SE_e = \frac{1}{2} U_e^T \mathbf{K}_e U_e \rho^p \tag{42a}$$

subject to:

$$\begin{gathered} \sigma_{prin,e} - \sigma_{Allow} \leq 0 \\ 0 \leq \rho_{\min} \leq \rho_e \leq 1 \\ (\sum_{i=1}^{n} \rho_i v_i) * \bar{\rho} > 0 \end{gathered} \tag{42b}$$

4.2.1 Sensitivity analysis

The sensitivity analysis is performed by considering the first derivative of the fundamental equation is given in Eq. (43) below. Derivative of the strain energy is:

$$\frac{\partial SE_e}{\partial x} = 0.5\, U_e^T \mathbf{K}_e U_e (p)(\rho^{p-1}) \tag{43}$$

5. Problems

5.1 Static analysis of a two dimensional plate carrying in-plane loading

A rectangular plate structure as shown in Fig.8 with dimensions starting from 0.5 mm to 8.5 mm along x-axis and starting from -1.73333 mm to +1.7333333 mm along y-axis is considered. The structure is as shown in Fig.8. The plate is meshed using eight numbers six node hexagon elements as shown in Fig.9. The material properties are the Young's modulus of elasticity is 200 GPa and the Poisson's ratio is 0.3. The six node hexagon elements are also known as honey beehive elements. The boundary conditions and load positions are kept the same. The six supports are provided as shown. Six point loads equal to 1 N are applied as shown. The hexagon elements have one edge in common. The structure is analyzed and the resulting nodal displacements were found. The stress at the centroid of each element is calculated. The total number of nodes is 30 and total number of hexagon elements is eight. The nodal displacements are found to be symmetrical. The stresses are found to be symmetrical. The maximum nodal displacement is found to be -1.399 x 10^{-05} mm. The maximum stress is found to be 0.76 MPa.

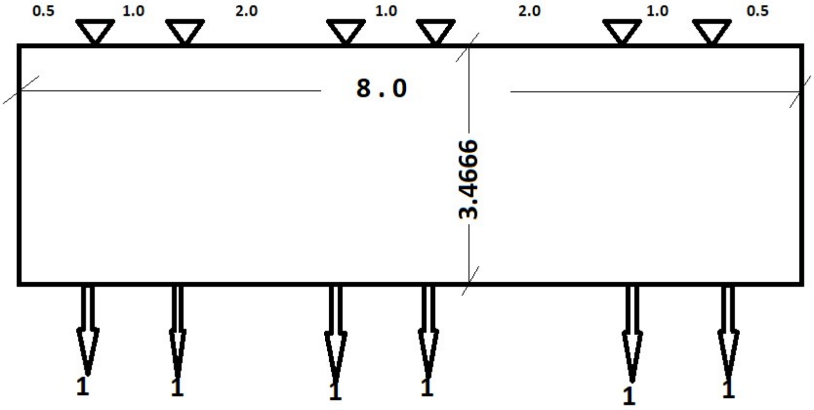

Fig. 8. The rectangular plate which is the initial domain

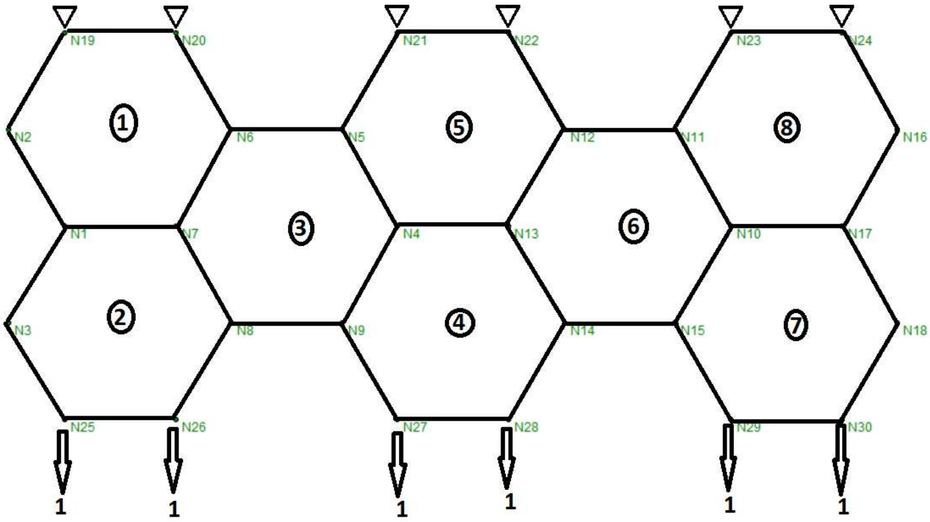

Fig. 9. The hexagon mesh using 6node hexagonal beehive elements

5.1.1 Analyzing using four-node quadrilateral element

The domain is analyzed in Marc Mentat® using first-order four node quadrilateral elements and the loading and boundary conditions are applied. The entire domain is meshed using 2916 nodes and 2800 elements. The Young's Modulus of elasticity is taken as 200 GPa and the Poisson ratio as 0.30. The analysis is performed in plane stress condition. The maximum Y-displacement is found to be -3.34951 x 10^{-05} mm.

The table of comparison between the maximum nodal displacements when the domain is meshed using first-order four node quadrilateral elements and six node hexagon elements is given in Table 2. The results clearly show that the design domain analyzed using Hex6 elements shows that the maximum nodal displacement is less than the maximum nodal displacement obtained when the design domain is meshed using quad4 elements. This is primarily due to the fact that the geometry of the hexagon elements is strongly interlocking. Let the side of the polygon be equal. The perimeter of the hexagonal element is more than a quadrilateral element and hence the shear strength is higher. The area within the boundary of the element is higher for hexagonal element and hence the bending strength is higher than the quadrilateral element. As a result, the nodal displacements of the mesh having hexagonal elements are less than the nodal displacements when quadrilateral elements are used.

Table 2. The maximum nodal displacements using quad4 and Hex6 mesh

	Using quad4 mesh	Using Hex6 mesh
Maximum nodal displacement	-3.34951 x 10^{-05} mm	-1.39974 x 10^{-05}

5.2 Topology optimization of plates carrying in-plane loading

5.2.1 Topology optimization of continuum plate using 6N hexagon elements carrying symmetrical in-plane loading and symmetrical supports

A two-dimensional plate of size 29 x 13.86666 is discretized into 143 numbers 6N hexagon elements, 18 numbers four node quadrilateral elements, 18 numbers 3 node constant strain triangle elements. The total number of nodes is 340. The Young's modulus of elasticity of the material is equal to 200 GPa and the Poisson's ratio is 0.3. The material density of the plate is taken as 7800 kg/m^3. The isoperimetric shape functions are used in the formulation of the stiffness matrix. The plate is supported at four nodes, two nodes at each end as shown in Fig.10. Four point loads of magnitude 1N each are applied symmetrically as shown in Fig. 10.

The hexagonal elements interlock each other better than the conventional quadrilateral elements. The static analysis has shown that the maximum nodal displacements when the domain is meshed using hexagonal elements are less than the maximum nodal displacements obtained when the quadrilateral elements are used to discretize and analyze the same domain.

Maximum nodal displacements using H6 mesh = -3.0922227924826331 x 10^{-005} mm

Maximum nodal displacements using Q4 mesh = - 5.04663 x 10^{-05} mm (Using Marc Mentat ®)

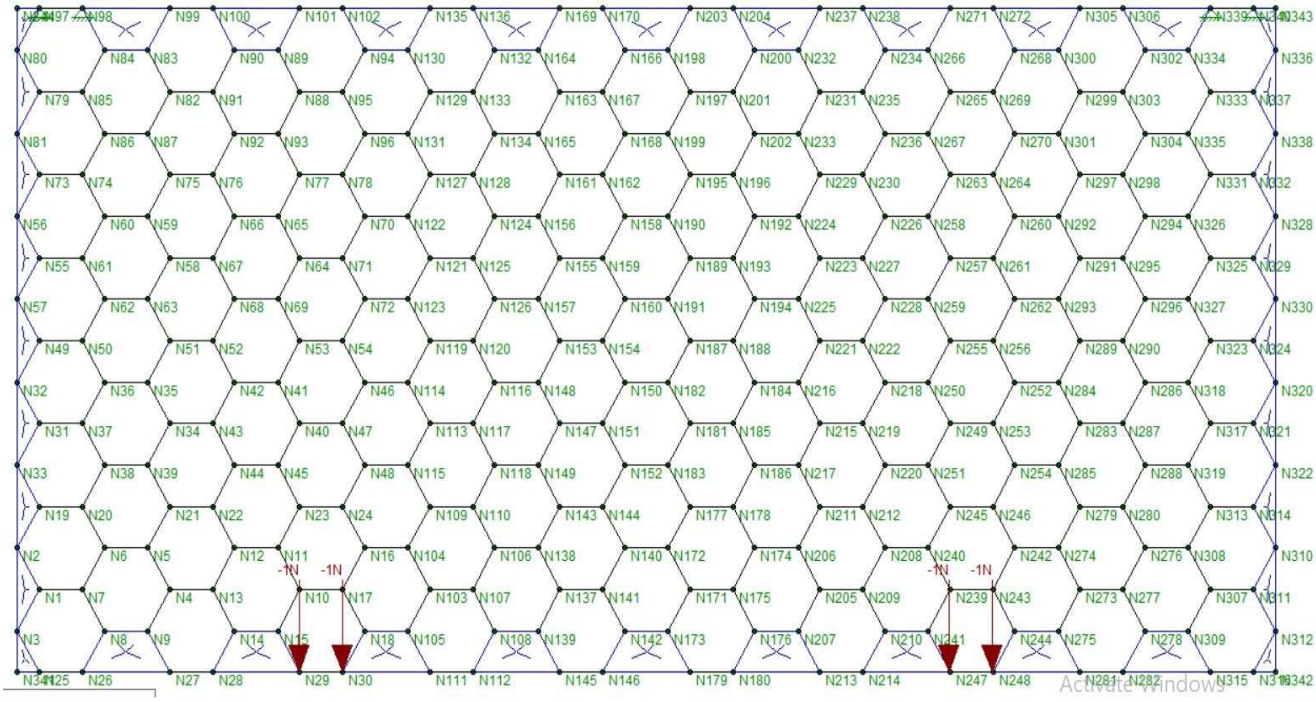

Fig. 10. The plate discretized using 6node hexagon elements, 4node quadrilateral elements, 3node constant strain triangular elements

Figure 11 shows the distribution of material after topology optimization using Firefly algorithm. The number of elements in the optimal distribution carrying material is 33 hexagonal elements out of 143 hexagonal elements in the initial domain, which is equal to 23.046% of the initial domain. The stresses were calculated at the centroid of each element and were found to be within the permissible limits. The nodal displacements were calculated at each node along both the degrees of freedom and were found to be within the permissible limits. The distribution is similar to the distribution obtained using conventional elements such as four node quadrilateral elements. The distribution of the elements shows that the elements are edge connected and can carry moment and shear force. The arrangement of elements is aligned curved as the geometry of the hexagon goes by.

5.3 Topology optimization of thin shell structures carrying out-of-plane loading

5.3.1 Optimizing the strain energy of a thin roof shell fixed at all the four corners of the structure

A shell roof surface having a radius of 25m and length of 50 m is fixed at all the four corner supports as shown in Fig.12. All the degrees of freedom are constrained to zero at these four corner supports. The shell roof is discretized using six node hexagonal elements into 605 elements and 1312 nodes. The Modulus of Elasticity is equal to 4.32e5 MPa and Poisson's Ratio is equal to 0.10. A point load of 10 N acting vertically downwards is applied at every node. The vertical axis is taken as the Z axis and the horizontal plane is XY plane. The permissible stress in the material is taken as 200 MPa and the permissible displacement is taken as 5 mm [24, 25].

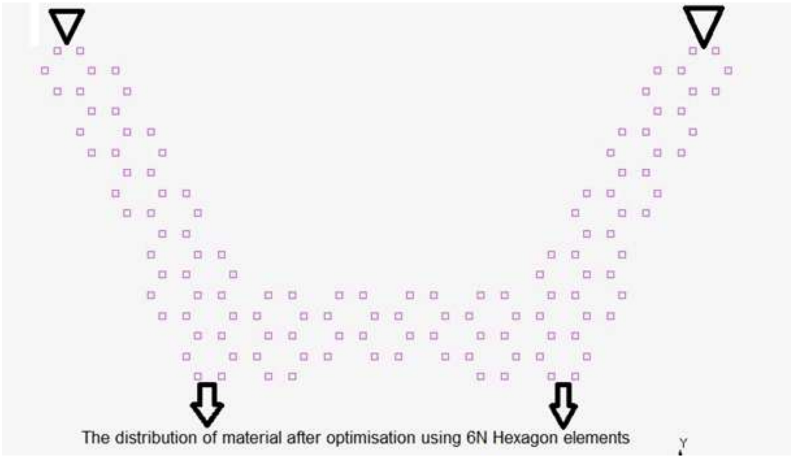

Fig. 11. The distribution of material on topology optimization using hexagon elements

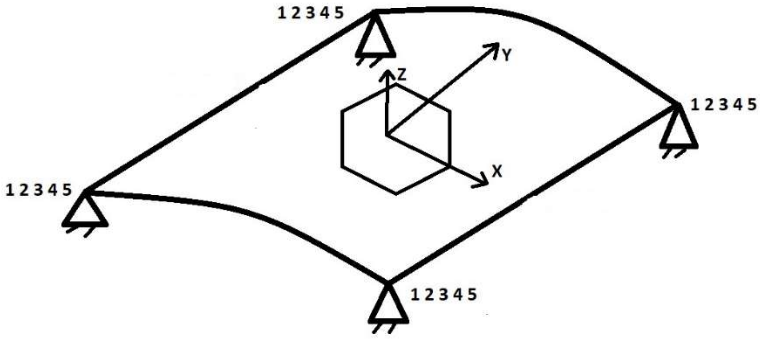

Fig. 12. The design domain having fixed supports at the four corners

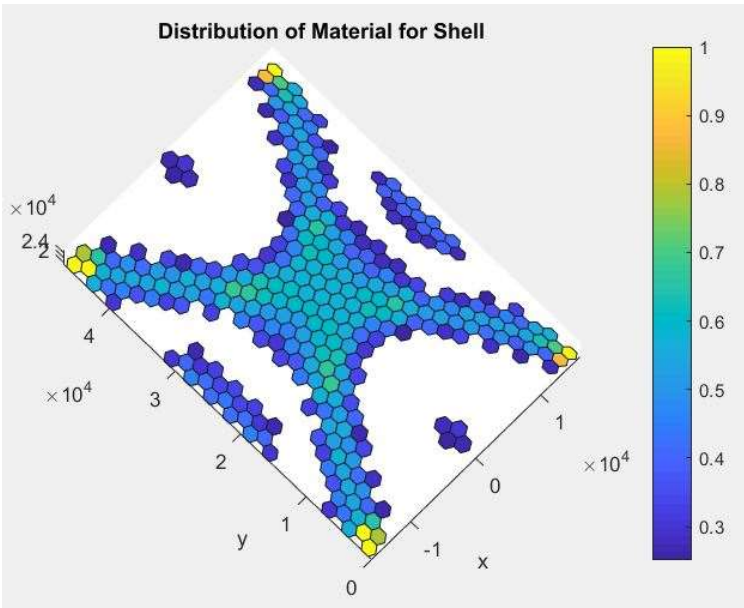

Fig. 13. The distribution of material for the thin shell after optimization

The hexagonal mesh is well-connected with each element having an edge in common. The hexagonal mesh is arranged in sequence of alternative rows of 20 elements and 19 elements per each row. A grid is prepared to show the element numbers which are connected to each other. This grid clearly shows the element numbers in each row and the neighboring elements for each element which are connected with an edge in common.

The thickness of the shell is taken as 0.25 x 10^3 mm. The number of six node hexagon elements is 605 and the number of nodes is 1312 having five degrees of freedom each. The Young Modulus of elasticity is taken as 4.32 x 10^5 MPa and the Poisson ratio is taken as 0.10. The shell carries a point load of 10N per node acting vertically downwards along the z-axis. The four corners of the shell with the node numbers 1, 20, 1293, 1312 are fixed. The penalization factor for the stiffness matrix is equal to 2. The filter radius is set as 2. The move parameter is taken as 0.30. The stabilization factor is 0.80. The final volume of the material is 30% of the initial volume of the shell. The lower limit to the Lagrange multiplier in optimality criteria is 0 and the upper limit is taken as 1x 10^{20}. The difference is set equal to 1 x 10^{-9}. The cutoff relative density is taken as 0.25.

The optimal distribution of material after 16 iterations is as shown in the Fig.13. Fig.14 shows the distribution of material obtained by Gullian [26]. The distribution of material obtained using six node hexagon is similar to the distribution of material obtained using quadrilateral elements. Fig.15 shows the variation of strain energy for each iteration.

The graph showing the strain energy on Y-axis and the iteration number on X-axis is as shown in Fig.15. The optimal distribution of the material shows that few elements carry material. The thickness of the shell can be increased for these elements and all the remaining elements can have lesser thickness. The hexagon grid can be provided to increase the stiffness of the structure. The total amount of the material required to build the structure can be saved. The structure is then analyzed to check for the maximum stress produced and the maximum nodal displacement.

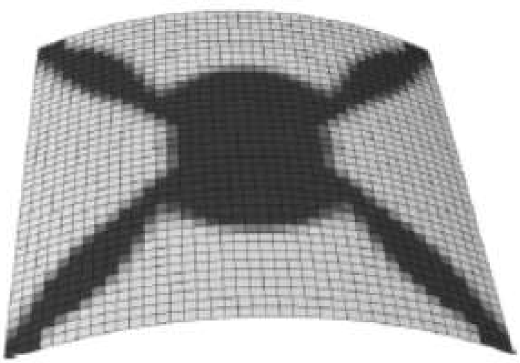

Fig. 14. Guillian solved a similar plate problem using TIMP using quad4 elements [26]

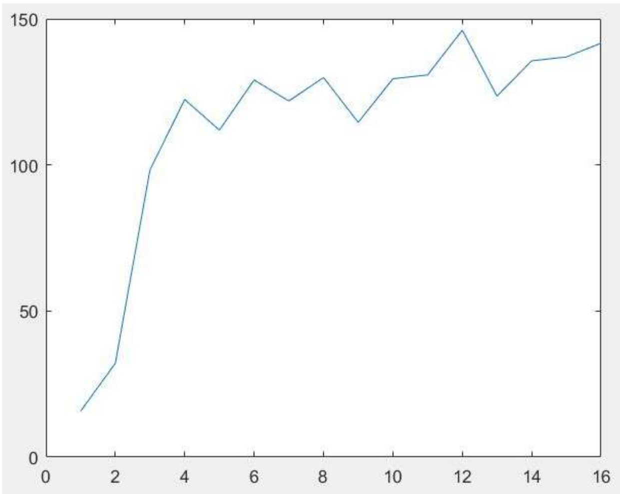

Fig. 15. The variation of Strain Energy for each iteration during the optimization process

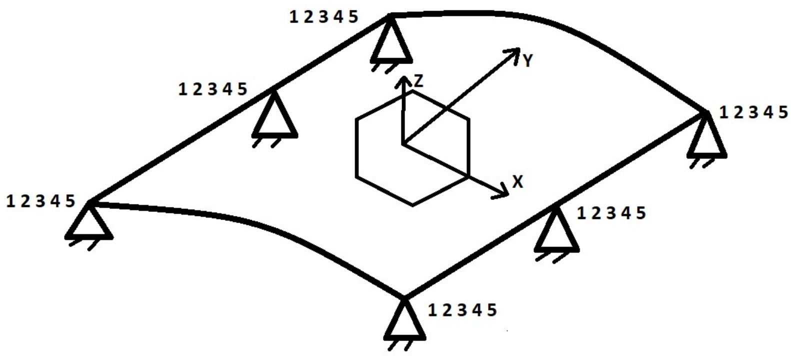

Fig. 16. The design domain having fixed supports at the corners at center of the long edge

5.4 Optimal design of stiffeners of a shallow roof shell fixed at four corners of the roof and at the mid-point center of long edge

The shell surface has a base of 2000 mm by 1500 mm [27] The longer sides are straight and the shorter sides are raised by 20.895mm as shown in the Fig.16. The calculations on the chord length of the curve are as shown in the Appendix A.

The thickness of the shell is taken as 1 mm. The number of six node hexagon elements is 605 and the number of nodes is 1312 having five degrees of freedom each. The Young Modulus of elasticity is taken as 1 x 10^7 MPa and the Poisson ratio is taken as 0.10. The shell carries a point load of 10N per node acting vertically downwards along the z-axis. The four corners of the shell and the center node along the long edges are fixed. The penalization factor for the stiffness matrix is equal to 2. The filter radius is set as 2. The move parameter is taken as 0.30. The stabilization factor is 0.80. The final volume of the material is 30% of the initial volume of the shell. The lower limit to the Lagrange multiplier in optimality criteria is 0 and the upper limit is taken as 1x 10^{20}. The difference is set equal to 1 x 10^{-9}. The cutoff relative density is taken as 0.25.

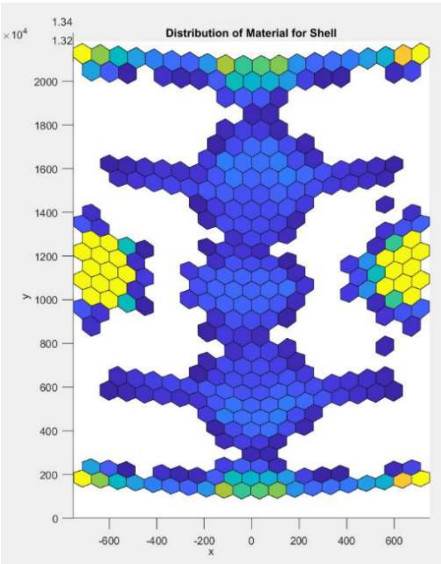

Fig. 17. (a) The present distribution

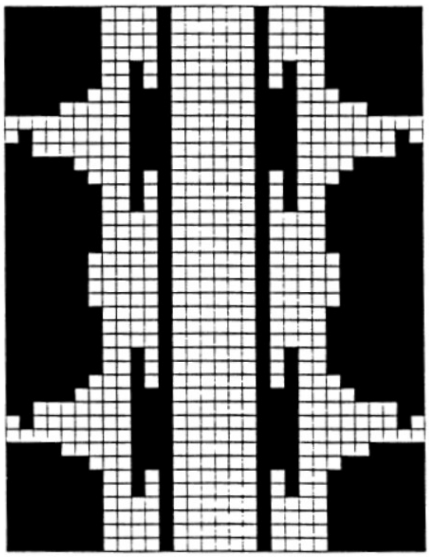

Fig. 17. (b) The distribution by Hae [27]

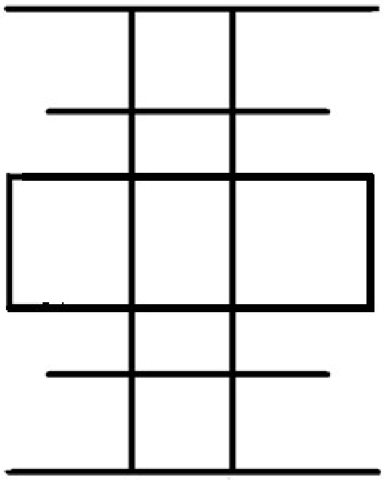

Fig. 17. (c) Line sketch showing the Design of Stiffeners using the output of optimization

The hexagon mesh exhibits patch behavior. The shear bond between the elements is stronger as the length of the element boundary more than the length of the boundary for a quadrilateral element and hence the hexagon mesh exhibits higher value of shear strength leading to a lump patch behavior.

The optimal design of stiffeners by GEA Fu as shown in Fig. 17(b) does not have connectivity of the material. The distribution of stiffeners obtained using hexagon elements has good connectivity of the material over the output obtained by GEA Fu as shown in Fig. 17(a). The optimal design includes both longitudinal and transverse members as stiffeners as shown in Fig.17(c) to increase the strength of the roof shell. The graph showing the variation of on Y-axis and iteration on X-axis is as shown in the Fig.18.

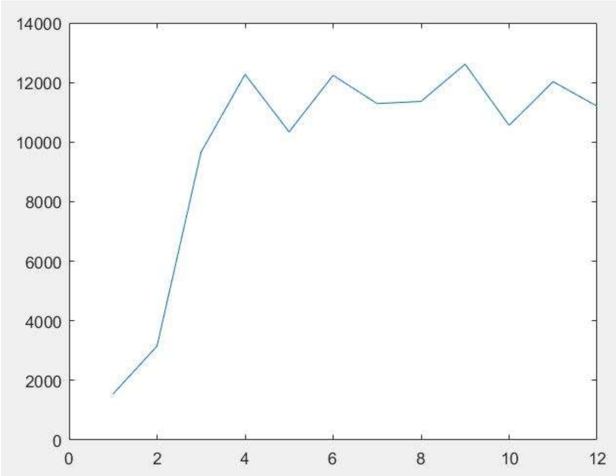

Fig. 18. The graph with strain energy on y-axis and iteration number on x-axis

6. Conclusions

The hexagonal structure of the element is from nature and is considered to be one of the strongest arrangements of unit cells. The honey bee hive is one such example. In this study, the rational fraction type shape functions are used and a few problems are analyzed and the results presented here. The rectangular domain is meshed using six node hexagon elements carrying in-plane loading. The results from the static analysis have clearly shown that the nodal displacements and centroidal stresses are symmetrical and the element is stable. The domain is meshed using first order four node quadrilateral elements in plane stress condition. The results clearly indicate that the maximum displacement obtained using six node hexagon elements is -1.399 x 10^{-05} mm and the maximum stress is found to be 0.76 MPa. The maximum nodal displacement obtained using first order four node quadrilateral element is -3.34951 x 10^{-05} mm. The rectangular domain is meshed using 340 nodes and 143 six node hexagonal elements. The topology optimization is performed using metaheuristic algorithms with minimal weight as the objective function. The optimal distribution of material clearly shows that the distribution is very similar to the distribution of material obtained using first order four node quadrilateral element. The topology optimization of the continuum domain has shown that the maximum displacements obtained when the hexagonal elements were used are less than the maximum displacements obtained when the quadrilateral elements were used. Maximum nodal displacements using H6 mesh = - -3.0922227924826331 x 10^{-005} mm. Maximum nodal displacements using Q4 mesh = - 5.04663 x 10^{-05} mm (Using Marc Mentat ®). The optimal distribution shows that the hexagonal elements interlock each other well and the distribution of material is strong when compared with the rectangular quadrilateral elements. The shear strength of the element is due to the length of the element measured along the boundary. The hexagon element has higher shear strength as the length of the element measured along the boundary is higher than for the quadrilateral element. The final distribution of material is 23.046% of the initial weight. The grid method is proposed in this paper to identify the elements in the neighborhood of each element to calculate the strain energy. The elements in the neighborhood are chosen as aligned along a sine curve. The topology optimization of thin roof shell structures is performed with strain energy as the objective function. The optimal distribution of material shows that the hexagonal elements exhibit strong interlocking nature. The optimal distribution of material obtained using hexagonal elements is similar to the optimal distribution of material obtained using quadrilateral elements. The fourth problem is to perform topology optimization using optimality criteria with strain energy as the objective function. The optimal distribution of material clearly shows that the stiffeners form a well-connected grid. The distribution using six node hexagon elements is improved over the final distribution obtained earlier in the literature. Hence, the hexagon mesh exhibits patch behavior with a group of few hexagon elements strongly linked with each other. The hexagon elements have higher shear strength along the edge connecting these elements.

6.1 Future study

The study can be extended to the design of reinforced cement concrete hexagonal roof shells with frequency optimization as the objective. The study can be useful to determine the optimal distribution of material for damping of structures subjected to loading.

Conflict of Interest

The authors declared no potential conflicts of interest with respect to the research, authorship and publication of this article.

Funding

The authors received no financial support for the research, authorship and publication of this article.

References

[1] S. Singh, *Optimal Integration Schemes for Polygonal Finite Element Method with Schwarz-Christoffel Conformal Mapping*, Master's Thesis, Indian Institute of Science, Bangalore, 2010.
[2] M. Ishiguro, K. Higuchi, Application of hexagonal Element Scheme in Finite Element Method to Three-Dimensional Diffusion Problem of Fast Reactors, *Journal of Nuclear Science and Technology*, 20(11), 1983, 951-960.
[3] M. Mehrenberger, L.S. Mendoza, C. Prouveur, E. Sonnendrucker, Solving the Guiding-Center model on a regular hexagonal mesh, *ESAIM: Proc.*, 53, 2016, 149-176.
[4] C. Talischi, G.H. Papulino, C.H. Le, Wachspress Elements for Topology optimization, Department of Civil and Environmental Engineering, University of Illinois at Urbana-Champaign, Proceedings of the *6th International Conference on Computation of Shell and Spatial Structures*, IASS-IACM, Cornell University, Ithaca, NY, USA, 2008.
[5] O. Verners, *Shape optimization of a Superelement of hexagonal Lattice Structure*, Riga Technical University, Modris Dobelis, Riga Technical University, 2010.
[6] T. Huang, Y. Gong, S. Zhao, Effective In-Plane Elastic Modulus of a Periodic Regular hexagonal Honeycomb Core with Thick Walls, *Journal of Engineering Mechanics*, 2018, 144(2), 06017019.
[7] R. Levy, W.R. Spillers, Optimal design for axisymmetric cylindrical shell buckling, *Journal of Engineering Mechanics*, 115(8), 1989, 1683.
[8] S.A. Falco, S.M.B. Alfonso, L.E. Vaz, Analysis and Optimal design of plates and shells under dynamic loads - II: optimization, *Structural and Multidisciplinary Optimization,* 27, 2004, 197-209.
[9] D. Khoza, *Topology optimization of plate-like structures*, Master of Engineering Thesis, University of Pretoria, 2005.
[10] I. Mekjavić, Buckling analysis of concrete spherical shells, *Tehnički Vjesnik*, 18(4), 2011, 633-639.
[11] T. Yin, H.F. Lam, Dynamic Analysis of Finite Length Circular Cylinder shells with a circumferential surface crack, *Journal of Engineering Mechanics*, 139(10), 2013, 1419-1434.
[12] A.I. Harb, K.C. Fu, Analysis and optimal design of spherical shells under axisymmetric loads, *Journal of Engineering Mechanics*, 116(2), 1990, 324-342.
[13] A. Aswini, G. Ramakrishna, Computer aided analysis of cylindrical shell roof structure using Matlab, *International Journal for Trends in Engineering & Technology*, 23(1), 2017, 6-10.
[14] S. Ahmad, B.M. Irons, O.C. Zienkiewicz, Analysis of Thick and Thin Shell Structures by Curved Finite Elements, *International Journal for Numerical Methods in Engineering*, 2, 1970, 419-451.
[15] K. Kant, R. Singh, Shell Dynamics with three dimensional degenerate finite elements, *Computers & Structures*, 50(1), 1994, 135-144.
[16] M.L. Bucalem, K.J. Bathe, Finite Element Analysis of Shell Structures, *Archives of Computational Methods in Engineering*, 4(1), 1997, 3-61.
[17] D. Visy, S. Adany, Local Elastic and Geometric Stiffness Matrix for the Shell element Applied in cFEM, *Periodica Polytechnica Civil Engineering*, 61(3), 2017, 569-580.
[18] V. den Boom, *Topology optimization Including Buckling Analysis*, Master of Science Thesis, Delft University of Technology, 2014.
[19] B. Archana, K.N.V. Chandrasekhar, T.M. Rao, A study on parameters of Firefly algorithm to perform Topology optimization of Continuum structures - II, *i-manager's Journal on Structural Engineering*, 6(1), 2017, 16-27.
[20] X.S. Yang, Firefly algorithms for multimodal optimization, *Lecture Notes in Computer Sciences*, 5792, 2009, 169-178.
[21] X.S. Yang, Firefly algorithm, Levy flights and global optimization, in *Research and Development in Intelligent Systems XXVI* (Eds M. Bramer, R. Ellis, M. Petridis), Springer London, 2010, 209-218.
[22] A. Baghlani, M.H. Makiabadi, M. Sarcheshmehpour, Discrete Optimum Design of Truss Structures by an Improved Firefly Algorithm, *Advances in Structural Engineering*, 17(10), 2014, 1517-1530.
[23] Y.W. Siu, B.S.L. Lai, F.W. Wang, Z.H. Zhou, S.L. Chan, Optimization of Structures by the Optimality Criteria Method, *HKIE Transactions*, 10(3), 2003, 48-53.
[24] K.J. Bathe, E.N. Dvorkin, A formulation of General Shell Elements - The Use of Mixed Interpolation of Tensorial Components, *International Journal for Numerical Methods in Engineering*, 22, 1986, 697-722.
[25] W. Altman, F. Iguti, A Thin Cylindrical Shell Finite Element Based on a Mixed Formulation, *Computers & Structures*, 6, 1976, 149-155.
[26] G. Yi, Y. Sui, TIMP method for topology optimization of plate structures with displacement constraints under multiple loading cases, *Structural and Multidisciplinary Optimization*, 53(6), 2016, 1185-1196.
[27] H.C. Gea, Y. Fu, 3-D Topology optimization using a Design Domain Method, *SAE Transactions: Journal of Passenger Cars*, 104(6): 1995, 1983-1989.

ORCID iD

K.N.V. Chandrasekhar https://orcid.org/0000-0003-3930-1196
S. Abdul Mohi https://orcid.org/0000-0002-8802-0502

Appendix A

A.1 Calculations for the radius of the shell curve

Problem:

Length of the arc = 1.5 m = 1500 mm.

Approximate method:

$$O_x = \frac{x(l-x)}{2R} \tag{A.1}$$

Arc definition:

$$\begin{aligned} &\frac{1500}{2\pi R} = \frac{\theta}{360} \Rightarrow R = \frac{85909.0909}{\theta} \\ &\theta = 20 \times 0.32 = 6.4^\circ, \quad R = 13423.295 \text{ mm} \\ &\text{Start angle} = 0.5 \times (180 - 20 \times 0.32) = 86.8 \\ &-749.309 \ \textit{to} \ 749.309 \\ &13423.295 - 13402.4 = 20.895 \text{ mm} \end{aligned} \tag{A.2}$$